Icequake-magnitude scaling relationship along a rift within the Ross Ice Shelf, Antarctica

Mong-Han Huang[1], Kathrine T Udell Lopez[2], and Kira G Olsen[3]

[1]University of Maryland, College Park
[2]University of Maryland
[3]Lamont-Doherty Earth Observatory of Columbia University

November 22, 2022

Abstract

Fractures within ice shelves are zones of weakness, which can deform on timescales from seconds to decades. Icequakes produced during the fracturing process show a higher *b-value* in the Gutenberg-Richter scaling relationship than continental earthquakes. We investigate icequakes on the east side of rift WR4 in the Ross Ice Shelf, Antarctica. Our model suggests a maximum icequake slip depth that is ~7.8 m below rift surface, where the slip area can only grow laterally along the fracture planes. We propose ductile deformation below this depth, potentially due to saturation of unfrozen water. We use remote sensing and geodetic tools to quantify surface movement on different time scales and find that the majority of icequakes occurred during falling tides. The total seismic moment is < 1% of the estimated geodetic moment during a tidal cycle. This study demonstrates the feasibility of using seismology and geodesy to investigate ice rift zone rheology.

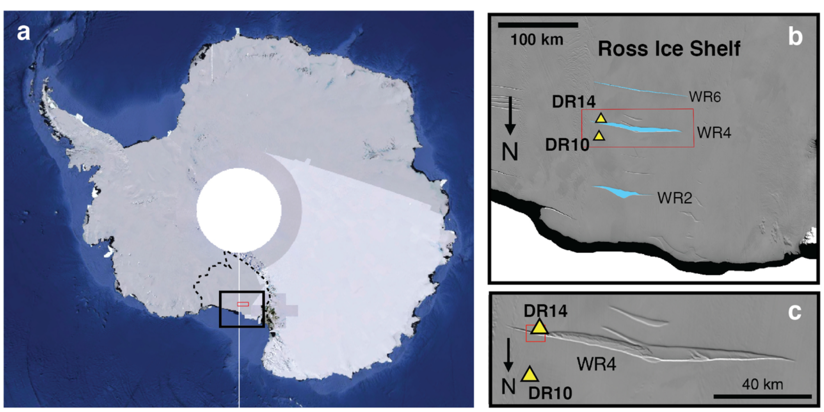

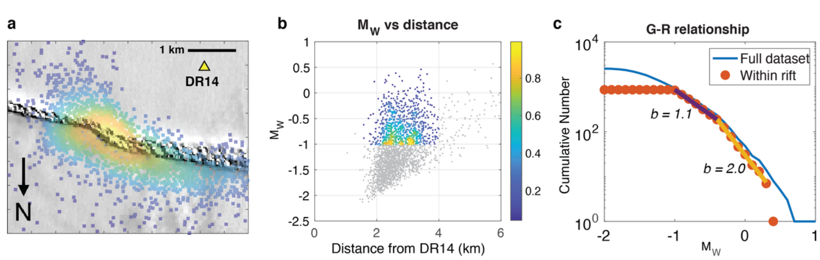

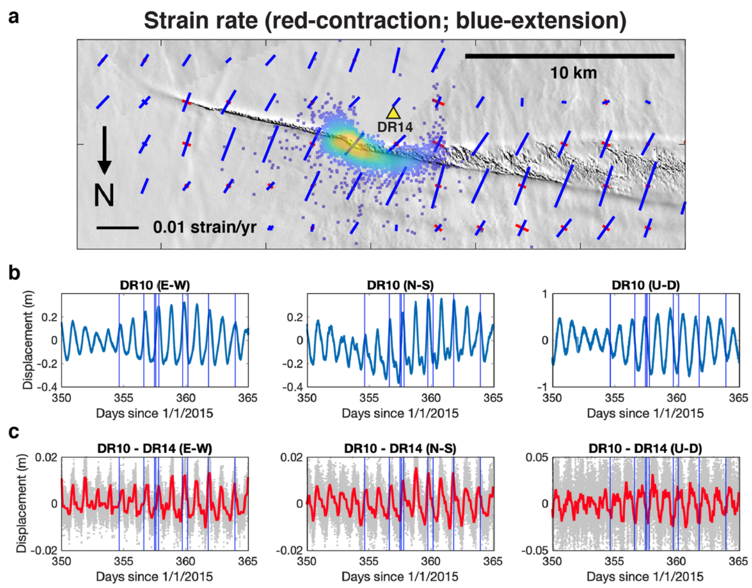
a
Strain rate (red-contraction; blue-extension)
10 km
DR14
N
0.01 strain/yr
b
DR10 (E-W)
DR10 (N-S)
DR10 (U-D)
Displacement (m)
Days since 1/1/2015
c
DR10 - DR14 (E-W)
DR10 - DR14 (N-S)
DR10 - DR14 (U-D)
Displacement (m)
Days since 1/1/2015

Icequake-magnitude scaling relationship along a rift within the Ross Ice Shelf, Antarctica

Mong-Han Huang[1], Kathrine Udell Lopez[1], Kira G. Olsen[1,2]
[1]Department of Geology, University of Maryland, College Park, MD, USA
[2]NASA Goddard Space Flight Center, Greenbelt, MD, USA

Abstract

Fractures within ice shelves are zones of weakness, which can deform on timescales from seconds to decades. Icequakes produced during the fracturing process show a higher *b-value* in the Gutenberg-Richter scaling relationship than continental earthquakes. We investigate icequakes on the east side of rift WR4 in the Ross Ice Shelf, Antarctica. Our model suggests a maximum icequake slip depth that is ~7.8 m below rift surface, where the slip area can only grow laterally along the fracture planes. We propose ductile deformation below this depth, potentially due to saturation of unfrozen water. We use remote sensing and geodetic tools to quantify surface movement on different time scales and find that the majority of icequakes occurred during falling tides. The total seismic moment is < 1% of the estimated geodetic moment during a tidal cycle. This study demonstrates the feasibility of using seismology and geodesy to investigate ice rift zone rheology.

Plain Language Summary

Fractures located on ice shelves are weak compared to the rest of the ice shelf. They deform over seconds to decades, and icequakes can be accompanied by their deformation. We find that tides, particularly falling tides, influence the frequency of icequake occurrence the most. We also find that small magnitude icequakes are a larger proportion of total icequakes when compared to the proportion of small magnitude continental earthquakes in relation to total global earthquakes. We test whether this proportion is due to the maximum depth estimated at 7.8 m below the surface of the rift zone by using satellite imagery, Global Navigation Satellite Systems (GNSS) measurements, and a seismometer located near a fracture on the Ross Ice Shelf. We propose that the rift zone below 7.8 m depth behaves as ductile deformation possibly due to saturation with unfrozen water, whereas the region above this depth is more prone to brittle fracture that can generate icequakes.

Key points:

1. Along the rift WR4 in the Ross Ice Shelf, evidence suggests most icequakes are driven by falling tides than long-term rift opening.
2. The b-value of icequakes in the Gutenberg-Richter relationship is generally greater than that for continental earthquakes.
3. We propose that the rift is water saturated ~7.8 m below the rift surface and prevents icequakes from occurring below this depth.

1. Introduction

The Gutenberg-Richter (G-R) relationship describes a relationship between the number of earthquakes in a region greater than a certain magnitude and that magnitude (*Gutenberg and Richter*, 1956). This relationship can be represented as:

$$\log_{10} N = a - bM_W, \tag{1}$$

where *a* represents the number of earthquakes when the moment magnitude (M_W) = 0, and *b* is the slope of the scaling relationship. For instance, when *b* = 1, there are 10^1 = 10 times more seismic events at a given magnitude than at the next lower magnitude value. On average, the b-value of global earthquakes is ~1 (*Lay and Wallace*, 1995), but for slow slip events and active volcanic regions, the b-value is close to 1.5 (*Ide et al.*, 2007; *Gomberg et al.*, 2016; *Rundle*, 1989). From global seismicity, the b-value appears to be around 1.5 for M_W > ~7 - 7.5 (*Pacheco et al.*, 1992). The break in the relationship is thought to be due to a presence of a “brittle-ductile transition zone”, a depth which slip cannot penetrate through, and therefore the slip area can only grow laterally.

The Ross Ice Shelf in Antarctica is the largest ice shelf on Earth (~525,000 km^2; Figure 1a,b). The ice shelf is a few hundred to over 1,000 meters thick and is moving toward the ocean with a speed from approximately 400 to 1,090 m/yr (ITS_LIVE dataset, *Gardner et al.*, 2019). About 170 km north from the grounding line, several rifts have been mapped within the Ross Ice Shelf (Figure 1b; *Walker et al.*, 2013; *Walker and Gardner*, 2019). Along Western Ross rift 4, or WR4, (Figure 1b,c), the ice velocities of the landward and seaward sides of the rift are different, causing a 10 - 50 m opening of the rift annually (*Walker and Gardner*, 2019). Using seismic data collected at station DR14 near WR4 between 2014 and 2016, *Olsen et al.* (2021) detected ~13,000 icequakes during a 25-month period. Among these icequakes, they were able to determine the magnitudes for ~2,500 icequakes. Based on the timing of the icequakes, they found a clear positive correlation between the onset of icequakes and tidally driven tensile stress, which is consistent with previous studies in a broader region on Ross Ice Shelf (e.g. *Olinger et al.*, 2019; *Chen et al.*, 2019). The G-R relationship within the rift zone shows a b-value between 1.2 and 1.5 (*Olinger et al.*, 2019; *Olsen et al.*, 2021), which is greater than similar magnitude continental earthquakes.

In this study, we investigate the higher b-value within WR4, estimate the energy required for the long-term rift zone opening, and compare the estimate with the cumulative seismic moment from the icequakes catalog created by *Olsen et al.* (2021). To accomplish this, we use both satellite imagery and Global Navigation Satellite System (GNSS) data to measure long-term surface strain rate and displacement during tidal cycles. We propose a maximum depth of icequakes within WR4 and a constant slip when the magnitude is greater than a certain value. This simple model can explain the higher b-value and predicts a reasonable slip value as well as stress drop. This work highlights the value of combining both seismologic and geodetic datasets for understanding Earth's polar ice sheets as well as icy worlds.

2. Data and Methods

2.1 Seismic Data

The seismic catalog used in this study was recently published by *Olsen et al.* (2021). The data was collected by a temporary seismic deployment spanning the Ross Ice Shelf during a 34-station campaign RIS/DRRIS project between November 2014 and December 2016 (*Bromirski et al*., 2015). *Olsen et al.* (2021) calculated the azimuth of 2,509 icequakes recorded at seismic station DR14 using surface-wave-arrival back azimuth method proposed by *Baker and Stevens* (2004). This method analyzes the polarization of recorded Rayleigh waves for back azimuth estimation using a single seismic station. To estimate distances between seismic station DR14 and icequake epicenters we handpicked the P and Rayleigh wave arrival times for these icequakes, then combined azimuth and distance calculations to locate this set of icequakes (Figure 2). The local magnitude (M_L) of each icequake was calculated using the maximum absolute displacement amplitude of each event, as described in *Olsen et al*. (2021).

2.2 Satellite Imagery & GNSS Data

To investigate long-term velocity and deformation on the Ross Ice Shelf, we adopt the horizontal movement and opening of WR4 estimated by *Walker and Gardner* (2019). We also use the

ITS_LIVE dataset to calculate surface strain rate near WR4 (Supplementary Text S1). This is an ice shelf surface velocity measurement based on satellite data (*Gardner et al.*, 2019). For short-term (diurnal) deformation, we use GNSS data to measure inter-tidal cycle displacements. Thirteen GNSS stations were temporarily deployed on the Ross Ice Shelf between November 2015 and early 2017 (*Bromirski and Gerstoft*, 2017). *Klein et al.* (2020) processed the high-rate (1-Hz) GNSS solutions from the 13 stations and characterized both short-term (sub-daily) and long-term (annual) displacements. Stations DR14 and DR10 are located on each side of WR4, with DR14 ~2 km and DR10 ~10 km away from WR4 (Figure 1b,c). DR10 has 2 years of continuous displacement measurements, whereas there is a data gap for DR14 during the winter season due to a lack of sunlight.

3. Results

3.1 Seismic Results

From the spatial distribution of the icequakes, there is a clear cluster of seismicity located along a bent segment of WR4 (Figure 2a). This bent segment is ~460 m in length and ~160 m in width (Figure S1). Although the uncertainty of icequake locations is high due to a single-station location technique, this result strongly suggests that the majority of located icequakes in this catalog occurred within the bend inside the rift zone. This finding is consistent with icequake locations at WR4 calculated by *Olinger et al.* (2019) using a multi-station location technique.

We find a clear increase in the minimum magnitude of icequake detection with distance from seismic station DR14 (Figure S2). For example, the minimum detection is approximately M_W -2 on the near side of WR4 relative to DR14, and M_W -1.2 on the far side. Although the icequake locations are not well constrained, there is a clear cluster of seismicity between 2 and 4 km possibly coming from the rift zone (Figure 2a,b). To fully capture the G-R relationship of the rift zone, we only consider icequakes within 4 km of distance from DR14. We also change the minimum magnitude cutoff until the icequake population density distribution becomes uniform, which is when $M_W > -1$ (Figure 2b). The G-R relationship from this subset of icequakes shows a clear change of slope when $M_W = -0.4$ (Figure 2c). Using a least square fit to the curves, the b-value is 1.1 between M_W -1 and -0.4, and 2.0 between M_W -0.4 and 0.3. We do not include M_W 0.4 in this calculation because there is only one icequake in this magnitude, which may not be representative of the distribution. We additionally plot the icequake G-R relationship of the near- and far-sides of WR4 and find consistent change of b-value at M_W -0.4 (Figure S3a).

3.2 Long-term (annual) deformation

Walker and Gardner (2019) found a rift opening rate between 10 and 50 m/yr along WR4. At the bent segment of WR4 (Figure 2a), the opening rate is ~10 m/yr. Since the width of WR4 here is 160 m, this bent segment opens ~6% per year. We calculated the principal strain rates and dilatation rate from the strain rate tensor on 500 m spacing grid points at WR4 (Figures 3a & S5). The result shows that the principal extension strain rate axes align perpendicular to the strike of WR4, even along the bent segment of WR4, implying low to negligible shear motion along the rift during long-term deformation (Figures 3a & S5).

3.3 Short-term (diurnal) deformation

GNSS stations DR10 and DR14 are collocated with the seismic stations (*Bromirski et al.*, 2015; *Bromirski and Gerstoft*, 2017). We adopt the displacement time series solutions from *Klein et al.* (2020). In a 20-day time window of one GNSS station, there is up to 0.5 m vertical displacement during diurnal tidal cycles (U-D in Figure 3b). In horizontal components, after removing the long-term trends, we find up to 0.4 m horizontal displacements during tidal cycles (E-W and N-S in Figure 3b). Although we are not able to directly estimate deformation within the rift, if we assume rigid motion of the ice shelf (i.e. negligible internal deformation), the majority of the internal deformation would occur within the rifts. We can therefore estimate the internal strain of WR4 near the bent segment by taking the differential displacement between DR10 and DR14, which is similar to the approach for the Nascent Iceberg also on Ross Ice Shelf (*Hurford and Brunt*, 2014). As shown in Figure 3c, the results indicate up to 0.015 m in horizontal and 0.03 m in vertical displacements with 60-sample moving average. Note that positive displacement in the north-south direction shows an increase in distance between the two GNSS stations during falling tides. The majority of the icequakes (vertical lines in Figure 3c) occurred during falling tides and is consistent with tidal patterns identified in *Olsen et al.* (2021).

4. Discussion

4.1 Energy budget associated with icequakes, long- and short-terms deformation

4.1.1 Seismic moment

We calculated the cumulative seismic moment based on the icequake catalog derived by *Olsen et al.* (2021). The scaling between M_L and M_W in *Olsen et al.* (2021) is based on *Munafò et al.* (2016) for small earthquakes (local magnitude M_L < 3):

$$M_W = \frac{2}{3}M_L + 1.15. \quad (2)$$

Following this, moment magnitude (M_W) is related to the seismic moment (M_o) (*Hanks and Kanamori*, 1979):

$$M_W = \frac{2}{3}\log_{10} M_o - 6.07, \quad (3)$$

where M_o is in the unit of N m. Comparing Equations 2 with 3, it suggests that M_L can directly scale with seismic moment for lower magnitude events when the instrument cutoff frequency is much lower than the corner frequency of the event (*Deichmann*, 2017). Although the scaling relationship is slightly different, similar results were found in Southern California (*Ross et al.*, 2016; *Staudenmaier et al.*, 2018) and Switzerland (*Bethmann et al.*, 2011). The cumulative seismic moment (Figure 4a) shows a significant seismic moment increase due to the largest M_W 1.5 event. If we remove the largest event for simple visual illustration, we find a clear difference in accumulation during summer and winter, where greater seismic moment accumulation is observed during austral wintertime (March-September). A plot of cumulative number of icequakes with time shows a similar pattern (Figure S3b). This result is consistent with the finding by *Olinger et al*. (2019) and *Chen et al.* (2019).

4.1.2 Long-term strain energy

To estimate the strain energy within the bent segment of the rift, we first determine the volume of the rift and the stress within the material. From visual inspection of the icequake locations (Figure 2a), it is reasonable to assume that the majority of the icequakes are from the bent segment of the rift. The thickness of the Ross Ice Shelf near WR4 is estimated to be ~300 m using shallow-ice radar echogram images (ROSETTA-Ice project; *Das et al.*, 2020). Assuming isostasy and the density of water = 1,030 kg/m^3 and ice = 917 kg/m^3, and the surface topography of the rift zone is ~20 m below the rest of the ice shelf (from the 2 m resolution digital elevation model [DEM] of the Worldview satellite imagery; Figure S1), the thickness of the rift zone is estimated as ~118 m. As a result, the volume of the bent segment is estimated as 8.7×10^6 m^3.

As described in Section 3.2, the long-term dilation rate is ~0.063/yr. The amount of stress required to maintain this dilation rate is estimated to be ~2×10^5 Pa, using a power-law relation between steady-state strain rate and deviatoric stress for Ross Ice Shelf (*Jezek et al.*, 1985). Assuming uniform strain rate within the rift, the annual strain energy is estimated as,

$$U = \frac{1}{2}\, V\, \sigma\, \dot{\varepsilon} = 8.8 \times 10^{7} Nm/yr, \tag{4}$$

where V is volume, σ is tensile stress required for the amount of strain rate, and $\dot{\varepsilon}$ is strain rate. This annual accumulated strain energy is equivalent to a M_W -0.77 event per day (orange line in Figure 4a). This amount of strain energy rate is clearly lower than observed seismic moment rate (blue line in Figure 4a). The observed icequakes are unlikely triggered by the long-term dilatation of the rift.

4.1.3 Short-term (Diurnal) tidal stress

As shown in Figure 3c, there is up to a few centimeters of displacement between stations DR10 and DR14. If we assume that deformation is within the rift, the peak vertical displacement shown in Figure 3c within the bent segment of WR4 is ~0.03 m during falling tide. As the tidal cycle is diurnal, which is significantly shorter than the Maxwell relaxation time of ice (~10^8 seconds), we assume elastic deformation in one tidal cycle. If we also assume slip (d) is the same across the entire rift wall, the slip area (A) as the length of the bent segment × thickness of WR4 ≈ 48,700 m^2, and the shear modulus (μ) of ice as 3.6 ×10^9 Pa (*Vaughan et al.*, 2016), the geodetic moment (M_{Go}) is: $M_{Go} = \mu\, A\, d =$ ~5.8 ×10^{12} N m (or M_W 2.4) every falling tidal. The largest observed icequake within the rift (M_W 0.4; Figure 2b,c) is only 0.09% of M_{Go}. This result suggests that the seismic moment observed here only represents small but routinely fracturing events on a small portion of the rift wall.

4.2 G-R scaling relationship of icequakes at WR4

To explore the b-value in the G-R relationship, we first discuss seismic moment and earthquake scaling. The seismic moment (M_o) is a measurement of the energy release of an event:

$$M_o = \mu\, A\, d. \tag{5}$$

Note Equation 5 has the same form as the geodetic moment. If μ of ice is constant, M_W scales with both A and d. As slip and slip area grow, d and A grow as a function of length (l) and length-square (l^2), respectively. As a result, when a length scale increases by an order for d and A, seismic moment (M_o) increases by 3 orders and M_W increases by a factor of two (Equation 3).

If there is a total area (S) that allows any slip to occur within S, the probability of an event with a certain slip area decreases with a larger event size as,

$$N_i = \frac{S}{A_i}\,, \tag{6}$$

where N_i is the number of events that can occur with a given slip area A_i. As a result, N_i and A_i are inversely proportional to each other, suggesting $N_i \propto l^{-2}$. Relating Equations 1, 3, and 5: $\log_{10} N = a - b[\frac{2}{3}\log_{10}(\mu A d) - 6.07]$, and therefore:

$$b \propto -\frac{3}{2}\,\frac{\log_{10} N}{\log_{10} Ad}. \tag{7}$$

Since $N_i \propto l^{-2}$, $A \propto l^2$, and $d \propto l$, $b = 1$.

Next, if there is a maximum depth (W_o) from ground surface where slip cannot penetrate through, slip area is represented as: $A = W_o\, L$, where L is the lateral length scale of fault. This implies $A \propto l$. If $d \propto l$, Equation 7 suggests that $b = 0.75$. Alternatively, *Romanowicz and Rundle* (1993) suggested that d could be invariant ($d \propto l^0$) when slip area reached W_o, and therefore $b = 1.5$. The G-R relationship of icequakes within the bent segment of WR4 indicates two b-values when $M_W > -1$ (Figure 2b). When M_W is between -1 and -0.4 the b-value is close to 1 and when $M_W > -0.4$, $b \approx 2$. Although the observed b-value is greater than 1.5, this pattern indicates a change of scaling relationship when $M_W \approx -0.4$ and implies that the icequake slip area reaches the maximum depth W_o when $M_W > -0.4$.

Stress drop ($\Delta\sigma$) is a change of shear stress due to a seismic event. Stress drop can be influenced by shear modulus (μ), slip area (A), and slip (d):

$$\Delta\sigma = C\,\mu \frac{d}{\sqrt{A}}\,, \tag{8}$$

where $C = \sqrt{5}$ for a rectangular slip area (*Pacheco et al.*, 1992), and $C = \frac{7\pi}{16}$ for a circular slip area (*Lay and Wallace*, 1995). From Equation 8, stress drop is a constant between different magnitudes when $b = 1$ (i.e. $A \propto l^2$ and $d \propto l$). If slip (d_o) is invariant ($d \propto l^2$) and slip area scales only with fault length ($A \propto l$), $\Delta\sigma$ scaling becomes:

$$\Delta\sigma = C\,\mu \frac{d_o}{\sqrt{W_o\,L}} \propto l^{-1/2}. \qquad (9)$$

This means stress drop decreases as fault length (and moment magnitude) increases.

4.3 Predicted slip and slip area of the largest event

The seismic moment of the largest icequake within the rift (M_W 0.4) is 5 × 10^9 N m. From Equation 5 and μ = 3.6 × 10^9 Pa, the slip and slip area product, $A\ d$ = 1.4 m^3. If we assume that the largest icequake has a slip equivalent to the largest differential displacement recorded by GNSS stations (d = 0.05 m; Figure 3c), then A = 28m^2. If we also assume the largest icequake corresponds to the slip of the entire bent segment (460 m; Figure 2a), then the width of the slip (in vertical direction) is area divided by length: $W_o = \frac{A}{L}$ = 0.6 m. We can then estimate the stress drop ($\Delta\sigma$) of this event, as $\Delta\sigma = \sqrt{5}\,\mu \frac{d}{\sqrt{A}}$ = 76 MPa. This value, however, is much greater than the tensile strength of ice estimated as 1.5 MPa, (*Podolskiy and Walter*, 2016), or 1.43 MPa within the temperature range -10 to -20°C (*Petrovic*, 2003). As a result, the amount of slip for this M_W 0.4 event is likely to be smaller than 0.05 m. From the G-R relationship (Figure 2b), if we consider the change of b-value as the critical condition when slip area cannot grow deeper, we can then assume that $\Delta\sigma$ = 1.5 MPa at M_W -0.4. In this scenario, $d \approx 0.0015$ m and $A \approx 61$ m^2. This suggests a 7.8 m × 7.8 m slip area.

Based on the analysis described above, we propose a depth similar to the "brittle-ductile transition" concept for Earth's crust. As shown in Figure 4b, for the Ross Ice Shelf this depth indicates a maximum depth where brittle failure could occur. Assuming the thickness of ice within the rift zone is ~118 m, as estimated in Section 4.1.2, this maximum brittle deformation depth is ~6.6% of the rift. This also suggests that the fault length of the largest M_W 0.4 icequake within the rift has a fault length of ~120 m with stress drop = 0.39 MPa.

Here we discuss potential explanations of this maximum slip depth. Although the permeability of ice is low (e.g. *Petrovic*, 2003), the porosity of the rift zone could be higher than the ice sheet due to the continuous rift opening (~0.063 per year). We then assume the rift zone is water saturated below sea level. By assuming isostasy, thickness of WR4 as 118 m, and the density contrast between water and ice, the depth to saturation is ~6.1 m below the rift surface, or ~5.6 m if the porosity of WR4 is 10%. This depth is shallower than the proposed brittle-ductile transition, but within the same order of magnitude. As air temperature is lower during wintertime, the unfrozen water level may be deeper at that time. This would imply a deeper brittle-ductile transition and allow for higher seismic production during winter months, as documented by *Olinger et al.* (2019) and observed within the catalog of icequakes examined here (Figures 4a & S3b).

4.4 Limitation of the analysis and future directions

High-resolution study of this rift is currently limited by instrumentation (single seismometer located ~5 km of WR4) as well as a shorter observation period. The seismic record examined here may not be of sufficient duration to capture a statistically representative number of higher-magnitude icequakes. Future deployment of additional seismic stations on the flanks of WR4 would enable higher-accuracy icequake locations, and calculation of focal mechanisms for larger icequakes. It would also allow for seismic verification of a maximum slip depth. Future work including higher density seismic and GNSS station deployments will significantly increase the detection level of icequakes, and we may even be able to measure surface displacement associated with larger icequakes. For example, we predict millimeter-level slip when the icequake $M_W > -0.4$. With high-rate GNSS stations deployed on both sides of the rift, they might detect mm-levels of seismic slip as well as the sense of motion.

5. Conclusions

We suggest that icequakes within WR4 are due to slip during diurnal falling tides. By using a combined seismic and geodetic dataset, we observe icequakes located within a bent segment of rift WR4 on the Ross Ice Shelf, Antarctica. An increase in the number of icequakes and cumulative seismic moment in winters implies more slip area available for icequake generation due to colder temperature within the shallower part of the rift zone. Long-term strain energy due to rift opening alone cannot explain the cumulative seismic moment of the icequakes. On the other hand, diurnal tidal stress can provide a sufficient amount of energy to generate icequakes. From the G-R relationship, we find a b-value greater than continental earthquakes. We adopt a simple scaling relationship to explain this high b-value, which suggests an existence of a maximum slip depth that is ~7.8 m below the rift surface. The proposed maximum slip is about 10% of the observed inter-tidal displacement between GNSS stations located on both sides of WR4, and the maximum slip depth is approximately the same length scale as the estimated water saturation depth of WR4.

Acknowledgements

The authors would like to thank Vedran Lekić, Nicholas Schmerr, Avinash Nayak, Victor Tsai, Catherine Walker, Sophia Zipparo, and Emilie Klein for their suggestions that significantly improves the quality of this work. This work is partially supported by NSF EAR-2026099 to M.-H. Huang. K.G. Olsen was supported by an appointment to the NASA Postdoctoral Program at the NASA Goddard Space Flight Center, administered by USRA under contract with NASA.

Data Availability Statement

The icequake catalog is included in the supplementary material and will be achieved in Zenodo after the peer review process. Seismic data used in this manuscript were collected through the NSF Office of Polar Programs project titled “Collaborative Research: Dynamic Response of the Ross Ice Shelf to Wave-Induced Vibrations” (network code XH; http://www.fdsn.org/networks/detail/XH_2014/). The GNSS data are available in *Klein et al.*, 2020. ITS_LIVE contains NASA products (https://its-live.jpl.nasa.gov/). The ROSETTA-Ice product is downloaded at (https://pgg.ldeo.columbia.edu/data/rosetta-ice). WorldView imagery used in this work is available to NSF- and NASA-funded researchers via the Polar Geospatial Center at the University of Minnesota.

References

Baker, G. E., & Stevens, J. L. (2004). Backazimuth estimation reliability using surface wave polarization. *Geophysical Research Letters*, *31*, L09611. https://doi.org/10.1029/2004GL019510

Bethmann, F., Deichmann, N., Mai, & P.M. (2011), Scaling Relations of Local Magnitude versus Moment Magnitude for Sequences of Similar Earthquakes in Switzerland. *Bulletin of the Seismological Society of America*; 101, 515–534. doi: https://doi.org/10.1785/0120100179

Bromirski, P. D., Diez, A., Gerstoft, P., Stephen, R. A., Bolmer, T., Wiens, D. A., et al. (2015). Ross Ice Shelf vibrations. *Geophysical Research Letters*, *42*, 7589–7597. https://doi.org/10.1002/2015GL065284

Bromirski PD and Gerstoft P (2017) Dynamic response of the Ross Ice Shelf to wave-induced vibrations 2015/2016, UNAVCO, Inc. GPS/GNSS Observations Dataset. doi: 10.7283/58E3-GA46.

Chen, Z., Bromirski, P., D, Gerstoft, P., Stephen, R. A., Lee, W. S., Yun, S., et al. (2019). Ross Ice Shelf icequakes associated with ocean gravity wave activity. *Geophysical Research Letters*, 46, 8893– 8902. https://doi.org/10.1029/2019GL084123

Das, I., Padman, L., Bell, R. E., Fricker, H. A., Tinto, K. J., Hulbe, C. L., et al. (2020). Multidecadal basal melt rates and structure of the Ross Ice Shelf, Antarctica, using airborne ice penetrating radar. Journal of Geophysical Research: Earth Surface, 125, e2019JF005241. https://doi.org/10.1029/2019JF005241

Deichmann, N. (2017), Theoretical Basis for the Observed Break in ML/MW Scaling between Small and Large Earthquakes. *Bulletin of the Seismological Society of America*, 107, 505–520. doi: https://doi.org/10.1785/0120160318

Ide, S., G. C. Beroza, D. R. Shelly, & T. Uchide (2007), A scaling law for slow earthquakes, Nature, 447(7140), 76–79, doi:10.1038/nature05780.

Gardner, A. S., M. A. Fahnestock, & T. A. Scambos, 2019 [update to 2021]: ITS_LIVE Regional Glacier and Ice Sheet Surface Velocities. Data archived at National Snow and Ice Data Center; doi:10.5067/6II6VW8LLWJ7.

Gomberg, J., A. Wech, K. Creager, K. Obara, & D. Agnew (2016), Reconsidering earthquake scaling, Geophys. Res. Lett., 43, doi:10.1002/ 2016GL069967.

Gutenberg, B. & Richter, C. Seismicity of the Earth and Associated Phenomena, 2nd edn, 310 (Princeton University Press. 1956).

Hanks, T.C., & H. Kanamori (1979), A moment magnitude scale, *J. Geophys. Res.*, *84*, 2348-2350.

Hurford, T. A., & Brunt, K. M. (2014). Antarctic analog for dilational bands on Europa. *Earth and Planetary Science Letters*, *401*, 275–283. https://doi.org/10.1016/j.epsl.2014.05.015

Jezek, K.C., Alley, R.B., & Thomas, R.H. (1985), Rheology of glacier ice, *Science*, 227, 4692, 1335-1337, https://www.jstor.org/stable/1695085

Klein E, Mosbeux C, Bromirski PD, Padman L, Bock Y, Springer SR, & Fricker HA (2020). Annual cycle in flow of Ross Ice Shelf, Antarctica: contribution of variable basal melting. Journal of Glaciology 66(259), 861–875. https://doi.org/10.1017/jog.2020.61

Lay, T. & Wallace, T. (1995), Modern Global Seismology, ISBN:012732870X, pp 521.

Munafò, I., Malagnini, L., & Chiaraluce, L. (2016). On the relationship between Mw and ML for small earthquakes. *Bulletin of the Seismo- logical Society of America*, *106*(5), 2402–2408. https://doi.org/10.1785/0120160130

Olinger, S. D., Lipovsky, B. P., Wiens, D. A., Aster, R. C., Bromirski, P. D., Chen, Z., et al. (2019). Tidal and thermal stresses drive seismicity along a major Ross Ice Shelf rift. *Geophysical Research Letters*, 46, 6644–6652. https://doi.org/10.1029/2019GL082842

Olsen, K. G., Hurford, T. A., Schmerr, N. C., Huang, M.-H., Brunt, K. M., Zipparo, S., et al. (2021). Projected Seismic Activity at the Tiger Stripe Fractures on Enceladus, Saturn, from an Analog Study of Tidally Modulated Icequakes within the Ross Ice Shelf, Antarctica. *Journal of Geophysical Research: Planets*, 126, e2021JE006862. https://doi.org/10.1029/2021JE006862

Pacheco, J., Scholz, C. & Sykes, L. (1992). Changes in frequency–size relationship from small to large earthquakes. *Nature* **355,** 71–73. https://doi.org/10.1038/355071a0

Petrovic, J.J., (2003). Mechanical properties of ice and snow, *Journal of Materials Science*, *38*, 1-6.

Podolskiy, E. A., & Walter, F. (2016). Cryoseismology. *Reviews of Geophysics*, *54*, 708–758. https://doi.org/10.1002/2016RG000526

Romanowicz, B., & Rundle, J.B. (1993) On scaling relations for large earthquakes. *Bulletin of the Seismological Society of America*, 83 (4): 1294–1297. doi: https://doi.org/10.1785/BSSA0830041294

Ross, Z.E., Ben-Zion, Y., White, M.C., & Vernon, F.L. (2016), Analysis of earthquake body wave spectra for potency and magnitude values: implications for magnitude scaling relations, *Geophysical Journal International*, 207, 1158–1164, https://doi.org/10.1093/gji/ggw327

Rundle, J. B. (1989), Derivation of the complete Gutenberg-Richter magnitude-frequency relation using the principle of scale invariance, *J. Geophys. Res.*, 94(B9), 12337–12342, doi:10.1029/JB094iB09p12337.

Staudenmaier, N., Tormann, T., Edwards, B., Deichmann, N., & Wiemer, S. (2018). Bilinearity in the Gutenberg-Richter relation based on ML for magnitudes above and below 2, from systematic magnitude assessments in Parkfield (California). *Geophysical Research Letters*, 45, 6887–6897. https://doi.org/10.1029/ 2018GL078316

Vaughan, M. J., Van Wijk, K., Prior, D. J., & Bowman, M. H. (2016). Monitoring the temperature-dependent elastic and anelastic proper- ties in isotropic polycrystalline ice using resonant ultrasound spectroscopy. *The Cryosphere*, *10*(6), 2821–2829. https://doi.org/10.5194/ tc-10-2821-2016

Walker, C. C., Bassis, J. N., Fricker, H. A., & Czerwinski, R. J. (2013). Structural and environmental controls on Antarctic ice shelf rift propagation inferred from satellite monitoring. *Journal of Geophysical Research: Earth Surface*, 118, 2354– 2364. https://doi.org/10.1002/2013JF002742

Walker, C. C., & Gardner, A. S. (2019). Evolution of ice shelf rifts: Implications for formation mechanics and morphological controls. *Earth and Planetary Science Letters*, 526, 115764. https://doi.org/10.1016/j.epsl.2019.115764

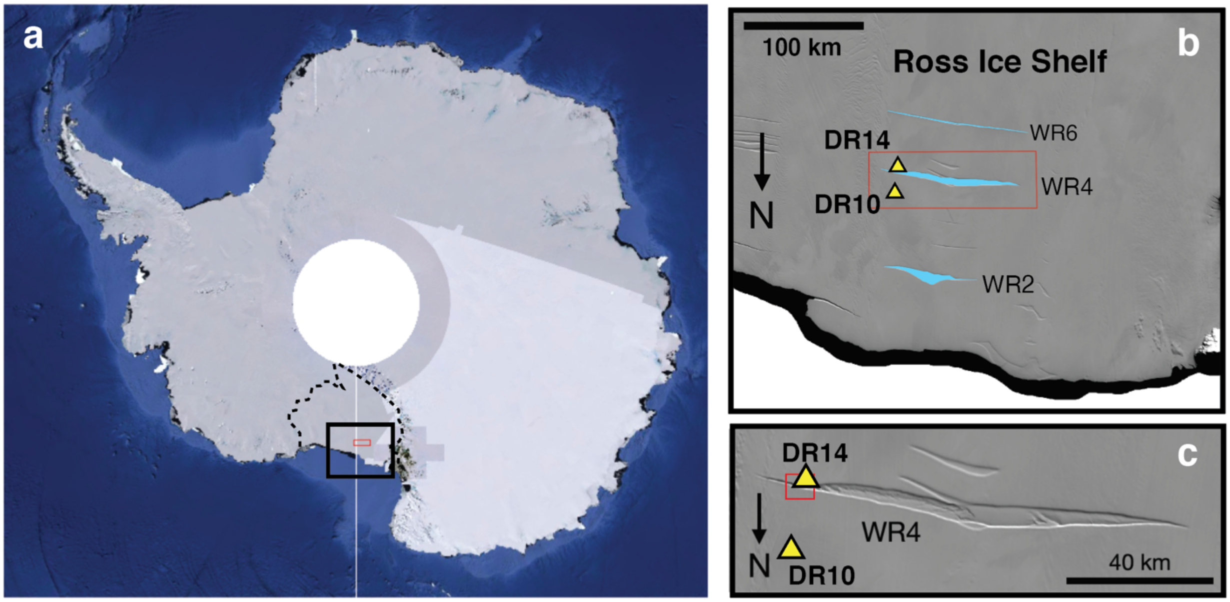

Figure 1. Study area. **(a)** View of Antarctica with the Antarctic Polar projection. The dashed polygon is the Ross Ice Shelf (Google Earth image) **(b)** North part of the Ross Ice Shelf. The light blue regions are the 3 major rift zones, WR2, WR4, and WR6. The yellow triangles in **b** and **c** are collocated broadband seismic and GNSS stations. The red rectangle marks the location of WR4 shown in **c**. **(c)** The red rectangle near DR14 is the figure outline of Figure 2a. The images in **b** and **c** are from MODIS.

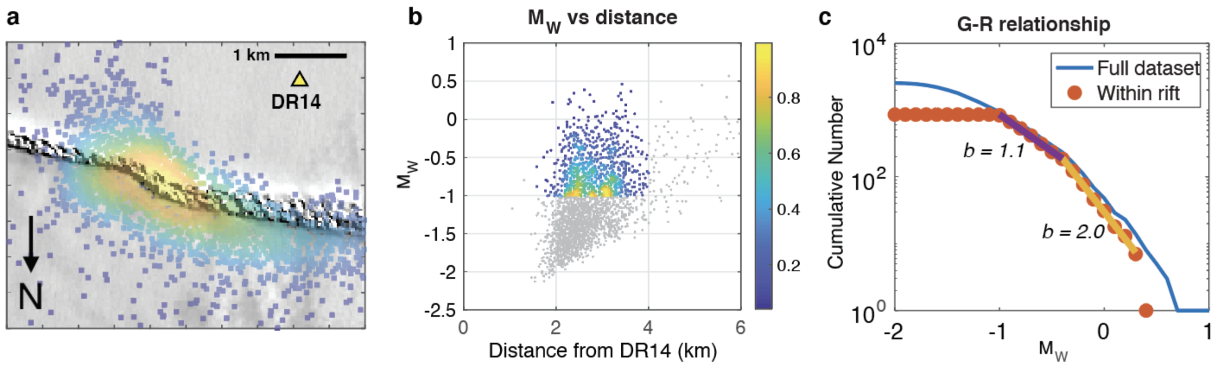

Figure 2. Seismicity and seismic scaling in WR4. **(a)** Seismicity on the east side of WR4 where the bent segment is located (location see Figure 1c). **(b)** Moment magnitude (*M_W*) vs distance. The grey dots denote the full icequake dataset examined in this paper. The colored dots denote icequakes within 4 km in distance from station DR14 and $M_W > -1$. The colors in **a** and **b** represent the normalized population density of icequakes. **(c)** Gutenberg-Richter (G-R) relationship of the icequakes. The blue curve is the full dataset, whereas the red circles are the colored events in **b**. The purple and orange lines represent the least square fits to the G-R relation when M_W is smaller and greater than -0.4, respectively.

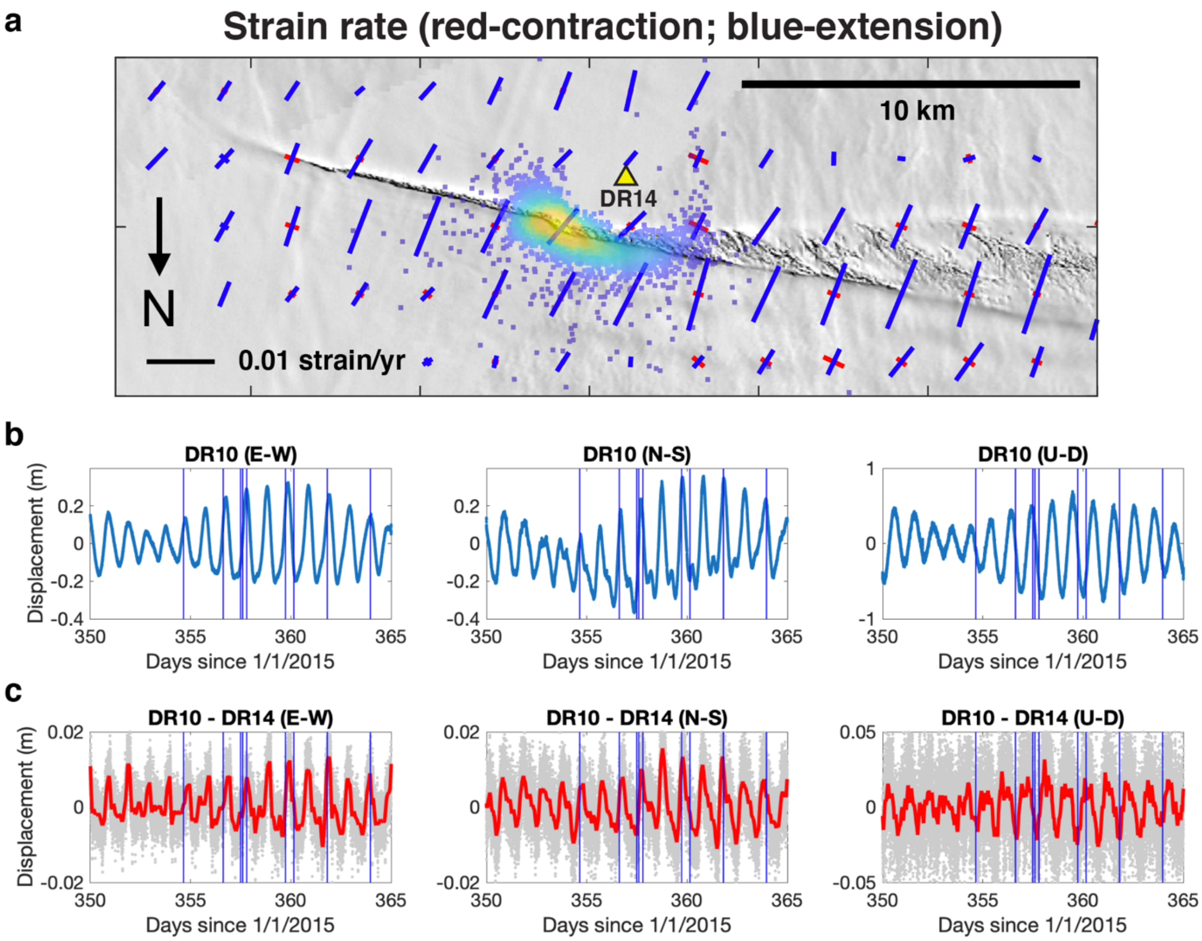

Figure 3. Surface deformation. **(a)** Principal strain rates calculated from long-term surface horizontal velocities (Figure S2). The direction of the bars indicate the principal axes orientations. **(b)** Surface displacement time series recorded from GNSS station DR10 (location see Figure 1b,c). E-W, N-S, and U-D represent east-west, north-south, and vertical displacements, respectively. Note the long-term horizontal displacement trends are removed. **(c)** Differential displacement time series between stations DR10 and DR14 (DR10 relative to DR14). The grey and red colors are the raw measurements and after 60-sample moving average, respectively. The blue vertical lines in **b** and **c** indicate individual icequake events.

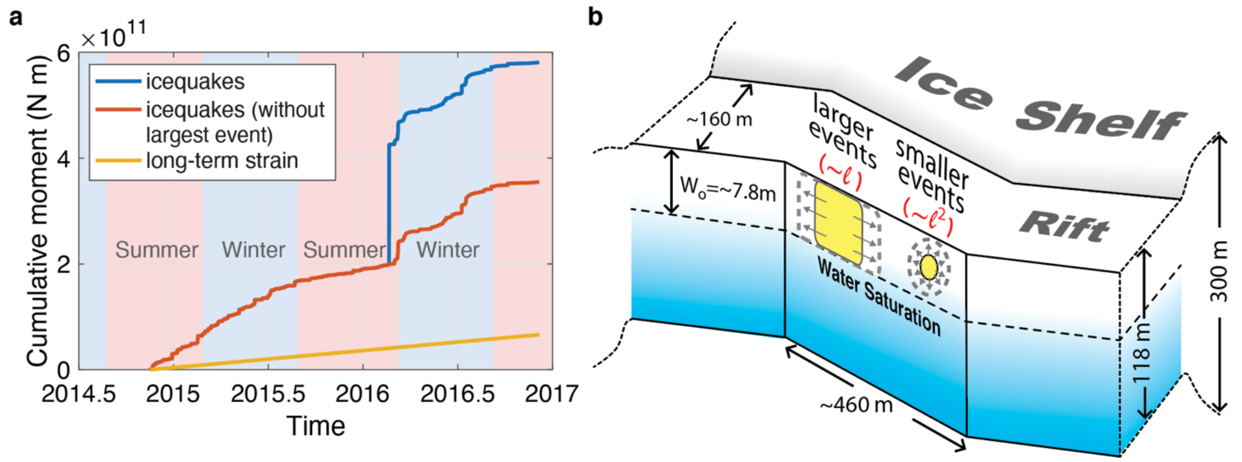

Figure 4. (a) Cumulative icequake seismic (red and blue) moment and the strain energy due to long-term rift opening (yellow). **(b)** Conceptual model of the icequake scaling. For smaller events, slip area grows with length square (l^2), but the slip area cannot grow past W_o, the brittle-ductile transition at ~7.8 m depth. Slip area grows laterally with a length scale (l) for events with magnitude M_W > -0.4.

Geophysical Research Letters

Supporting Information for

Icequake-magnitude scaling relationship along a rift within the Ross Ice Shelf, Antarctica

Mong-Han Huang[1], Kathrine Udell Lopez[1], Kira G. Olsen[1,2]

[1]Department of Geology, University of Maryland, College Park, MD, USA
[2]NASA Goddard Space Flight Center, Greenbelt, MD, USA

Contents of this file

Text S1
Figures S1 to S5

Additional Supporting Information

Dataset S1: Icequake catalog used in this study

Introduction

Text S1 describes the estimation of surface strain rate.
Figure S1 shows surface elevation of WR4.
Figure S2 shows the icequake locations and distance relative to station DR14.
Figure S3 shows the Gutenberg-Richter relationship and cumulative icequakes with time.
Figure S4 shows the ITS_LIVE dataset for WR4.
Figure S5 shows the surface strain rate using the ITS_LIVE dataset for WR4.

Supplementary Materials

Text S1. Estimation of surface strain rates using ITS_LIVE dataset

We download the dataset from the ITS_LIVE website (https://its-live.jpl.nasa.gov/). This data product includes horizontal velocities and their uncertainty estimates between 2015 and 2020. The original product is in geotif format, and the pixel size is about 450 m × 450 m. Figure S2 shows the velocities across WR4. We downsample the image to 2,700 m × 2,700 m pixel size using QGIS for the strain rate analysis. For strain rate, we first set a grid point array every 500 m in east-west and north-south directions, and then compute a 2 × 2 deformation tensor constrained from nearby velocity estimates, and then estimate the principal strain rate axes orientation and magnitude, respectively.

Although the ITS_LIVE product is based on multiple years of measurement, the data is still noisy when looking at a smaller spatial scale (e.g. sub-km). There are also additional double-rift features (most clear in the east-west component of Figure S2) that could be due to artifacts in image processing (*C. Walker*, *personal communication*). We try to reduce the data noise by considering velocity measurement from nearby pixels. We first estimate a mean velocity of the grid point from taking velocity estimates of the 8 neighboring pixels. We use a weighted least squares method with a linear equation to represent the mean velocity (in both east–west and north-south components) with the inverse of velocity uncertainty estimate, which is part of the original data products, for weighting.

To construct the 2 × 2 deformation tensor, we take the mean velocity of each grid point and estimate the relative velocity between grids and their distance:

$$\dot{\boldsymbol{\varepsilon}} = \begin{bmatrix} \dot{\varepsilon}_{xx} & \dot{\varepsilon}_{xy} \\ \dot{\varepsilon}_{yx} & \dot{\varepsilon}_{yy} \end{bmatrix} =$$

$$\begin{bmatrix} \dot{\varepsilon}_{xx} & \frac{1}{2}\left(\dot{\varepsilon}_{xy} + \dot{\varepsilon}_{yx}\right) \\ \frac{1}{2}\left(\dot{\varepsilon}_{yx} + \dot{\varepsilon}_{xy}\right) & \dot{\varepsilon}_{yy} \end{bmatrix} + \begin{bmatrix} 0 & \frac{1}{2}\left(\dot{\varepsilon}_{xy} - \dot{\varepsilon}_{yx}\right) \\ -\frac{1}{2}\left(\dot{\varepsilon}_{xy} - \dot{\varepsilon}_{yx}\right) & 0 \end{bmatrix},$$

where $\dot{\varepsilon}_{xx} = \frac{\partial V_E}{\partial x}$, $\dot{\varepsilon}_{yy} = \frac{\partial V_N}{\partial y}$, $\dot{\varepsilon}_{xy} = \frac{\partial V_E}{\partial y}$, and $\dot{\varepsilon}_{yx} = \frac{\partial V_N}{\partial x}$. V_E and V_N represent velocity in east-west and north-south, respectively. The first part of the right-hand side is the strain rate tensor, and the second part is the rotation rate tensor. We then calculate the eigenvalues and eigenvectors of the strain tensor for each grid point. The eigenvectors and eigenvalues correspond to the principal strain rate axes orientation and magnitude, respectively. The result of the principal strain rate is shown in Figure 3a, where red and blue represent contraction and extension rate, respectively. Figure S3 shows the principal strain rate, dilatation rate, and shear rate (projected to N5^{o}W) of WR4.

Supplementary Figures

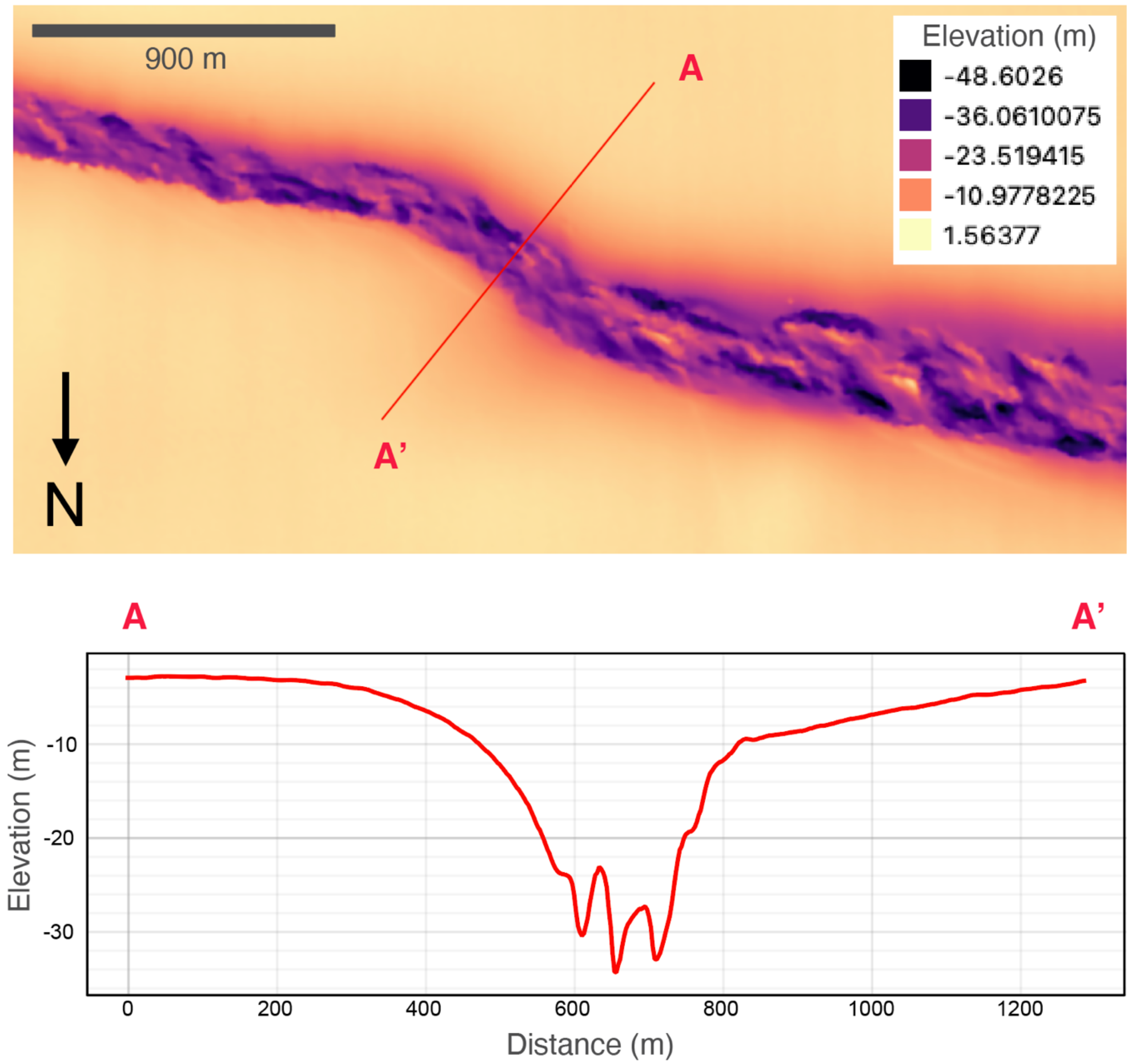

Figure S1. 2m resolution DEM and a rift-perpendicular elevation cross section from WorldView-2 satellite imagery. Color scale shows elevation in meters.

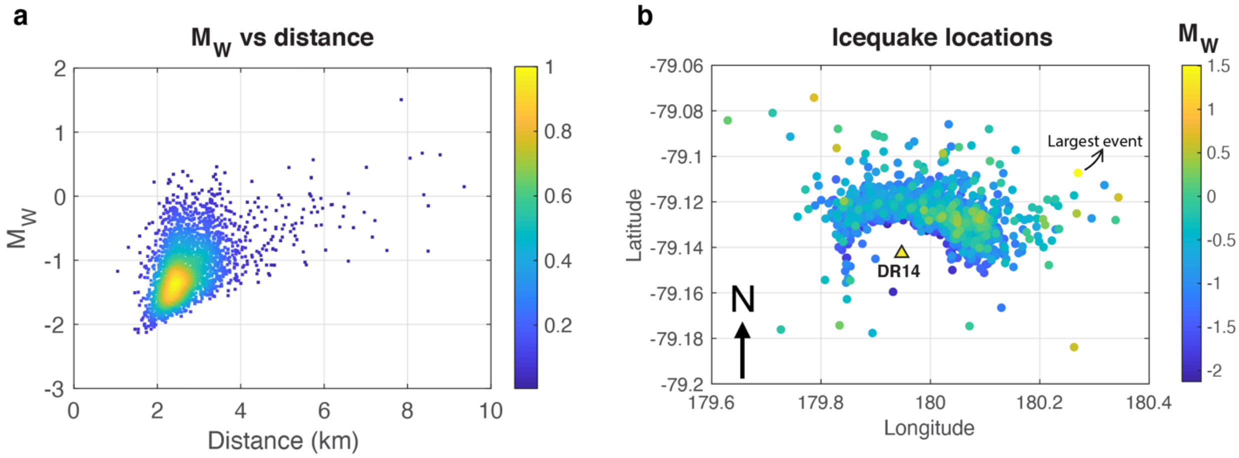

Figure S2. (a) Distance versus moment magnitude (M_W) plot. The color represents the icequake population density. The majority of the icequake are between 2 and 4 km distance from station DR14. **(b)** Map view of seismicity color coded with moment magnitude (M_W).

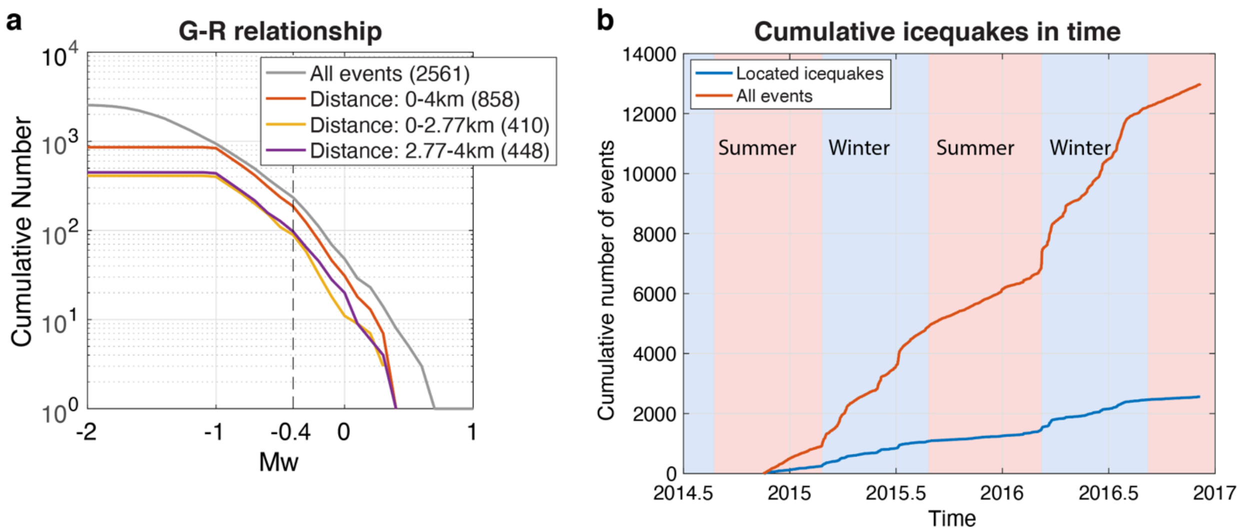

Figure S3. (a) Gutenberg-Richter relationship of all events (grey), WR4 (red), near- (yellow) and far- (purple) sides of WR4. The numbers in the legend represent number of icequakes. The vertical dashed line indicates M_W -0.4, where a change of slope (b-value) occurs. **(b)** Cumulative number of icequakes during observational period. There is higher seismicity production during Antarctic winter.

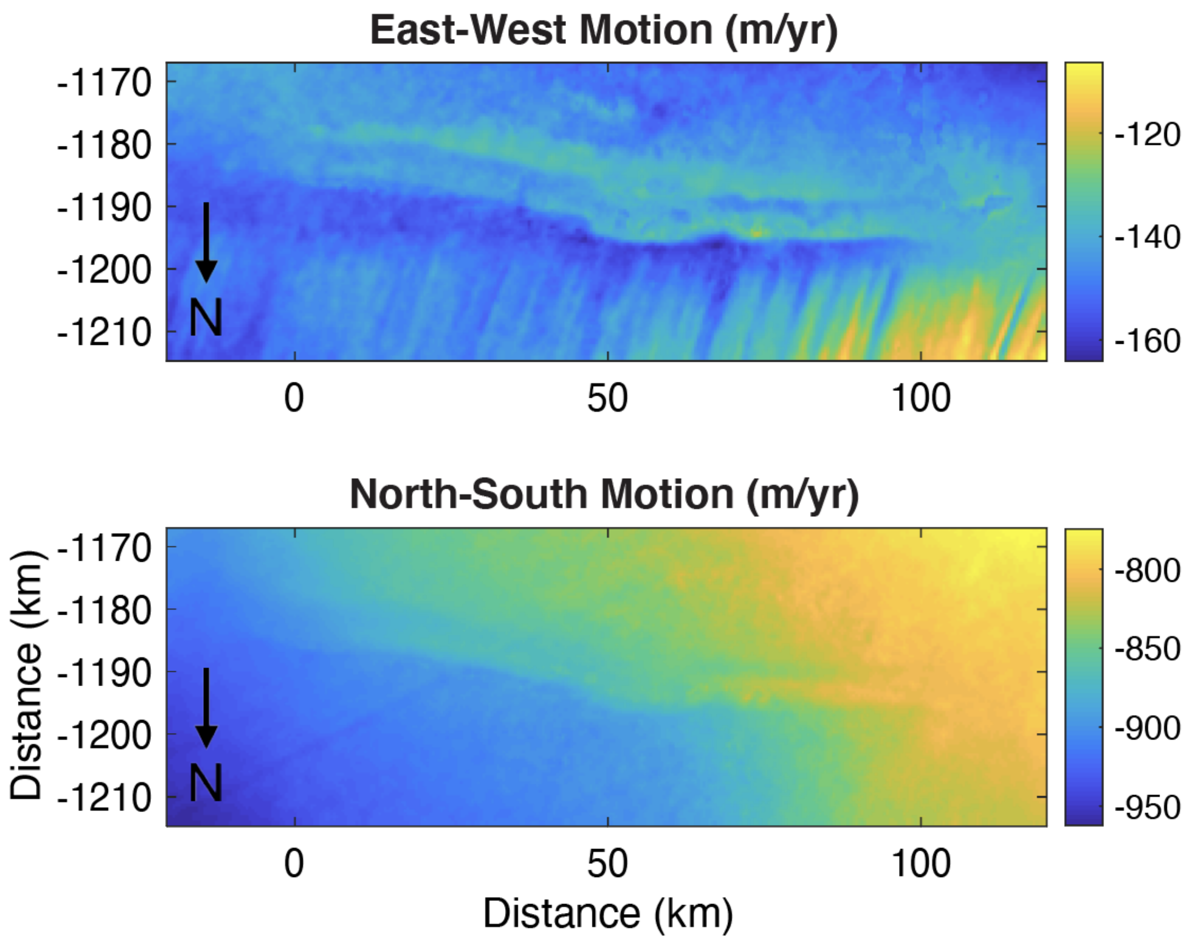

Figure S4. ITS_LIVE velocity in east-west and north-south direction.

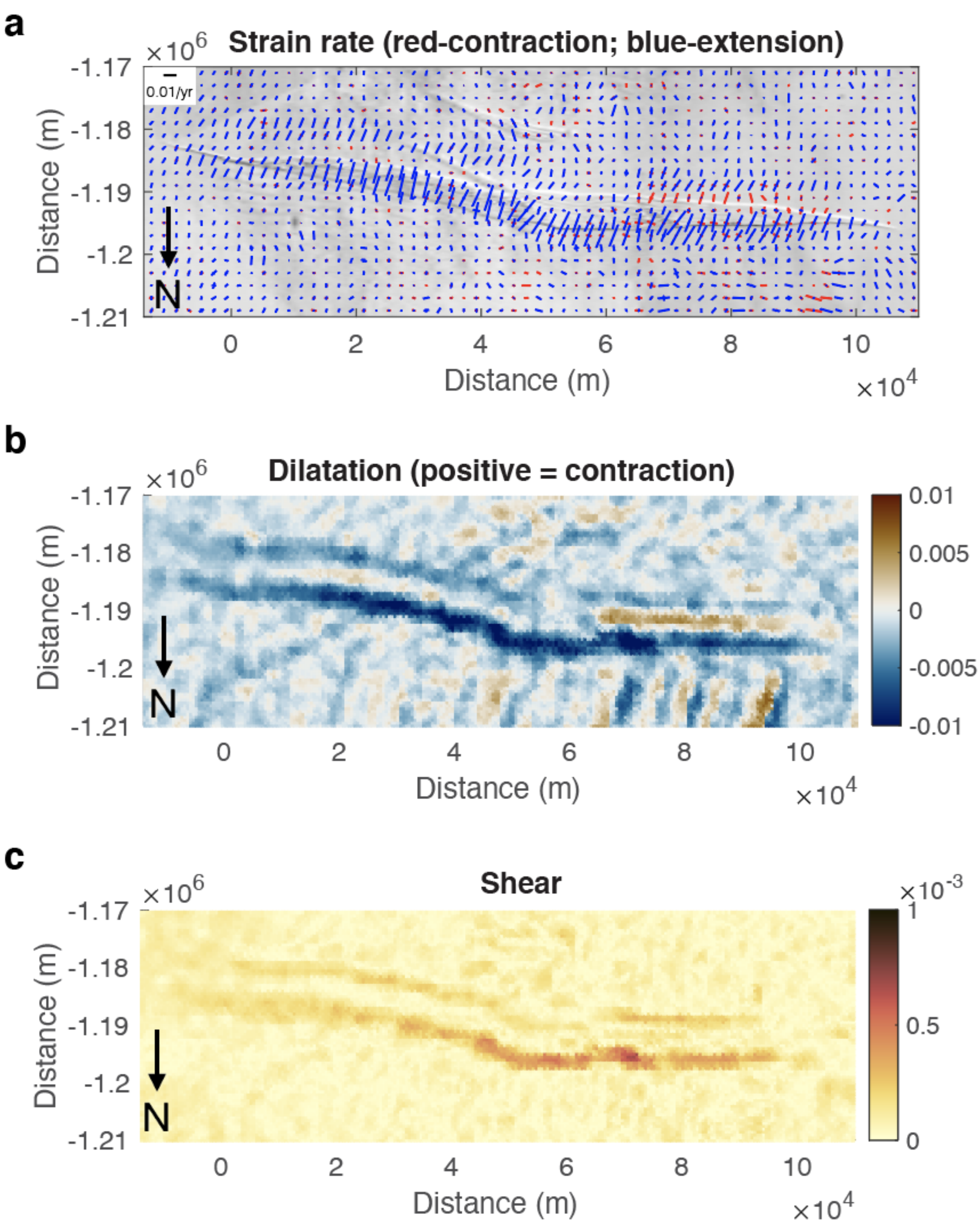

Figure S5. Strain rate along the full extent of WR4. **(a)** The blue and red bars represent extension and contraction rates, respectively, and the direction of the bars indicate the principal axes orientations. The background image is from Sentinel-2 imagery. **(b)** Dilatation rate. The blue and red colors represent extension and contraction, respectively. **(c)** Shear rate projected to N5°E, which represents the amount of shear motion along the east side of WR4.